Journal of ELECTRONIC MATERIALS, Vol. 45, No. 11, 2016
DOI: 10.1007/s11664-016-4366-z


# Characterization of Low-Melting-Point Sn-Bi-In Lead-Free Solders

QIN LI,[1,3] NINSHU MA,[2] YONGPING LEI,[1,4] JIAN LIN,[1] HANGUANG FU,[1] and JIAN GU[1]

1.—College of Materials Science and Engineering, Beijing University of Technology, 100 Ping Le Yuan, Chao Yang District, Beijing 100124, China. 2.—Joining and Welding Research Institute, Osaka University, 11-1 Mihogaoka, lbaraki, Osaka 567-0047, Japan. 3.—e-mail: li911206qin@163.com. 4.—e-mail: yplei@bjut.edu.cn

Development of lead-free solders with low melting temperature is important for substitution of Pb-based solders to reduce direct risks to human health and the environment. In the present work, Sn-Bi-In solders were studied for different ratios of Bi and Sn to obtain solders with low melting temperature. The microstructure, thermal properties, wettability, mechanical properties, and reliability of joints with Cu have been investigated. The results show that the microstructures of the Sn-Bi-In solders were composed of $\beta$-Sn, Bi, and InBi phases. The intermetallic compound (IMC) layer was mainly composed of $Cu_6Sn_5$, and its thickness increased slightly as the Bi content was increased. The melting temperature of the solders was around 100°C to 104°C. However, when the Sn content exceeded 50 wt.%, the melting range became larger and the wettability became worse. The tensile strength of the solder alloys and solder joints declined with increasing Bi content. Two fracture modes (IMC layer fracture and solder/IMC mixed fracture) were found in solder joints. The fracture mechanism of solder joints was brittle fracture. In addition, cleavage steps on the fracture surface and coarse grains in the fracture structure were comparatively apparent for higher Bi content, resulting in decreased elongation for both solder alloys and solder joints.

**Key words:** Sn-Bi-In, low-temperature solders, microstructure, melting properties, mechanical properties

## INTRODUCTION

With increasing application in electronic product industries, requirements on solders are also becoming more demanding. Lead-tin (Sn-Pb) solders have been widely employed in the microelectronics industry because of their low cost, moderate melting point, and good wettability and mechanical properties.[1,2] However, since lead is harmful to human health due to pollution of groundwater, development of lead-free solders has been an important task in the microelectronics packaging industry. Most commercial lead-free solders such as Sn-Ag-Cu have higher melting point (221.8°C) than eutectic lead-tin solder (183°C), and such increased melting temperature can reduce the reliability and functionality of temperature-sensitive components.[1] As a result, applications of these solders are limited to certain conditions. Therefore, a lower-temperature soldering process is required, and the development of reliable low-temperature lead-free solders is expected.

Researchers have proposed several solders as candidates, e.g., the Sn-Ag, Sn-Zn, Sn-In, and Sn-Bi systems.[1,3–6] It has been reported that the tensile strength, fatigue strength, and creep resistance of Sn-Ag solders are superior to those of Sn-Pb solders.[3,7] However, poor wettability and high melting point (about 220°C) limit their applications.[6] Sn-Zn solders have low melting point (198°C), close to that (183°C) of Sn-Pb solders. However, the poor

(Received November 6, 2015; accepted January 20, 2016; published online February 17, 2016)

antioxidation and corrosion resistance resulting from the active element Zn are their main problem.[4,6] Sn-In solders with low melting temperature are appropriate for temperature-sensitive components.[1] Meanwhile, Yang Shu et al.[8] investigated the characteristics of Sn/In nanosolders by changing the ratio of Sn to In. It was found that Sn/In nanosolders were composed of $InSn_4$ and $\beta$-Sn phases for less than 20 wt.% In, $InSn_4$ phase for 30 wt.% In, and pure In for more than 40 wt.% In. However, material cost is one of the principal limitations on large-scale application of Sn-In solders. Among these candidates, Sn-Bi-based solders have received much attention for replacement of Sn-Pb solders because of their low melting point, good wettability, good mechanical properties, and low cost.[5,9] However, Sn-Bi solders show brittle behavior both in the bulk and at the solder interface, and the mechanical properties may become worse due to Bi segregation at the $Cu/Cu_3Sn$ interface.[10,11] Therefore, a third element such as Ag, Sb, Ni, Cu, etc. has been added to try to improve the mechanical properties.[12–15] The elongation of Sn-58Bi alloys was significantly enhanced by addition of Ce element.[16] Addition of Cu could refine the grain size of the Bi-rich phase and improve the interface brittleness.[9] To date, several studies[17–21] have focused on research into the bulk properties of Sn-Bi-In solders and the effect of minor addition of In element to Sn-Bi solders. Yoon et al.[17] and Witusiewicz et al.[18] studied the phase equilibria and thermodynamic behaviors of the Sn-Bi-In system. The melting temperature, phase composition, and mechanical properties of fusible Sn-Bi-In ternary alloys have been investigated to obtain a material for a 72°C thermal actuator in an automatic sprinkler.[19] Besides, the melting temperature, thermal expansion, and microstructures of Bi-In-Sn solders with melting point of 61°C have also been studied.[20] Addition of 0.5 wt.% In and Ni was effective for suppressing IMC layer growth during thermal aging.[21] However, further studies on the bulk solder properties and microelectronic interconnection by solder joints need to be conducted.

In the present work, Sn-Bi-In solders were investigated to obtain low-temperature lead-free solders with melting point of around 100°C for use in devices such as fiber-optic gyroscopes. Although Sn-Bi-Cd solder has a eutectic point of 103°C[1] and is now being used in device soldering, substitute harmless solders need to be investigated due to the toxicity of Cd. In this study, the microstructures, thermal properties, wettability, and mechanical properties of Sn-Bi-In solders were investigated. The tensile properties and fracture characteristics of solder joints are also discussed.

## EXPERIMENTAL PROCEDURES

Based on our previous experimental work,[22] solders with low melting point of 100°C can be obtained by adding 12 wt.% In to Sn-Bi solders. Tin (99.9%), bismuth (99.9%), and indium (99.995%) were melted and mixed in alumina crucibles under

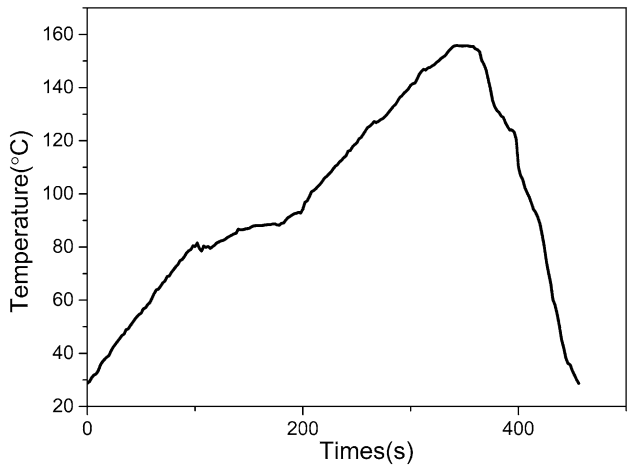


Fig. 1. Reflow process measured by thermocouple.

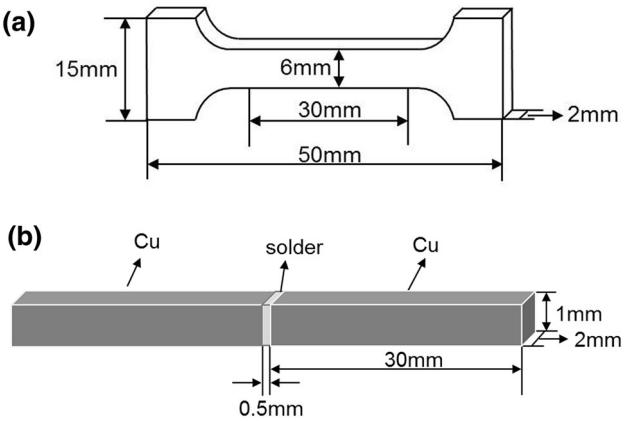


Fig. 2. Schematic illustration of mechanical properties testing: (a) tensile test for solder alloys and (b) tensile test for solder joints.

**Table I. Chemical composition of specimens (wt.%)**

| Alloy | Sn | Bi | In | Alloy | Sn | Bi | In |
|---|---|---|---|---|---|---|---|
| 1 | 38 | 50 | 12 | 4 | 47 | 41 | 12 |
| 2 | 41 | 47 | 12 | 5 | 50 | 38 | 12 |
| 3 | 44 | 44 | 12 | 6 | 53 | 35 | 12 |

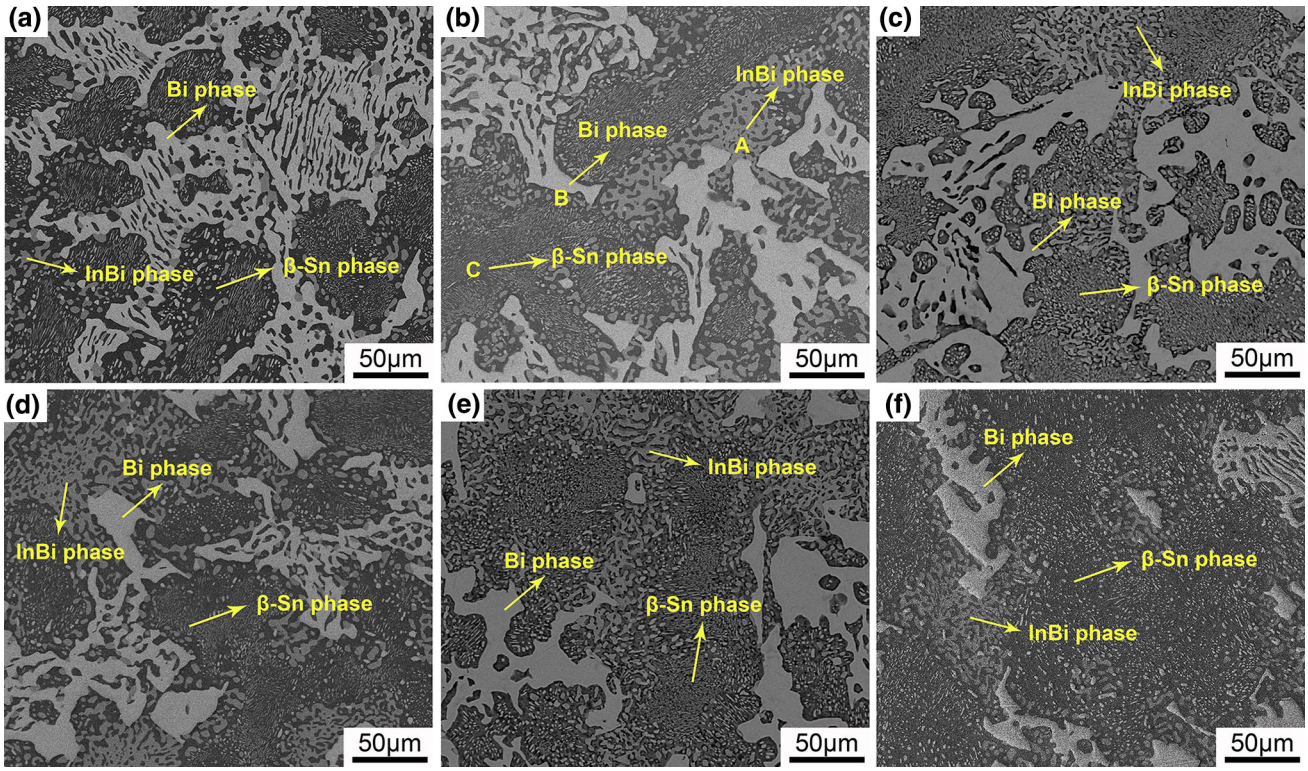


Fig. 3. Microstructures of solders: (a) 38Sn-50Bi-12In, (b) 41Sn-47Bi-12In, (c) 44Sn-44Bi-12In, (d) 47Sn-41Bi-12In, (e) 50Sn-38Bi-12In, and (f) 53Sn-35Bi-12In.

**Table II. EDX analysis for Fig. 3b: (A) InBi phase, (B) Bi phase, (C) β-Sn phase**

| | A | | B | | C | |
|---|---|---|---|---|---|---|
| **Element** | **wt.%** | **at.%** | **wt.%** | **at.%** | **wt.%** | **at.%** |
| Sn L | 4.95 | 6.80 | 7.65 | 11.95 | 73.58 | 79.60 |
| Bi L | 65.17 | 50.81 | 83.87 | 74.38 | 18.15 | 11.15 |
| In L | 29.88 | 42.39 | 8.48 | 13.67 | 8.27 | 9.25 |

$N_2$ at temperature of 400°C. The ingot was remelted two times to obtain a homogeneous mixture. Table I presents the chemical compositions of the specimens. The reflow process of solder joints is shown in Fig. 1, as measured by a thermocouple. The samples were preheated between 80°C to 90°C for 100 s, and the holding time above liquidus temperature was 188 s.

To study the microstructures of the solders and solder joints, optical microscopy, scanning electron microscopy (SEM), energy-dispersive x-ray spectroscopy (EDX), and x-ray diffraction (XRD) analysis were used. For microstructural analysis, specimens were ground to a smooth surface, followed by polishing with 0.3-$\mu$m $Al_2O_3$ powder. Phase identification was carried out using an x-ray diffractometer operated at 30 mA and 40 kV with Cu $K_\alpha$ radiation at diffraction angle $2\theta$ from 20° to 80° and scan speed of 2°/min. The thickness of intermetallic compound (IMC) layers was determined using ImageJ analysis software. Since the IMC layer is too thin, its thickness could not be measured directly. This thickness was therefore determined using the measured length and the section area based on a SEM image. To obtain a reliable thickness for the IMC layer, five specimens for each solder were prepared and ImageJ analysis software was employed.

Melting properties of solders were investigated by differential scanning calorimetry (DSC); all the samples for DSC were about 20 mg. The heating from 40°C to 170°C was controlled at a rate of about 10°C/min, and the measurement was performed two times in argon protective atmosphere. Wetting experiments complied with GB/T11364-2008. Samples and copper substrates (50 mm × 50 mm ×

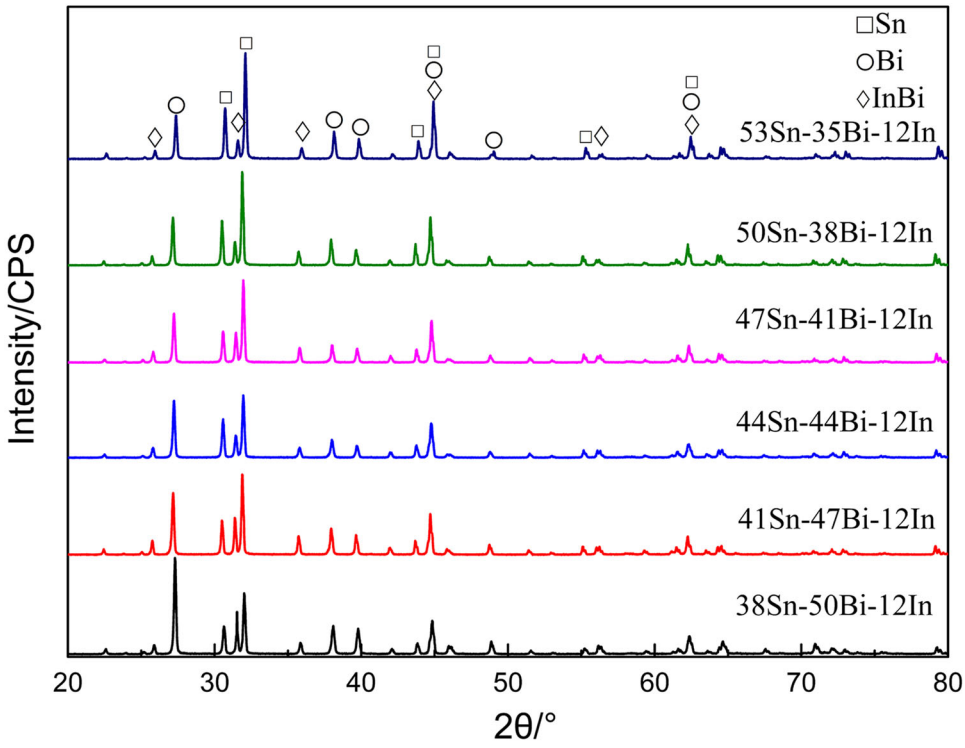


Fig. 4. XRD profiles of Sn-Bi-In solders.

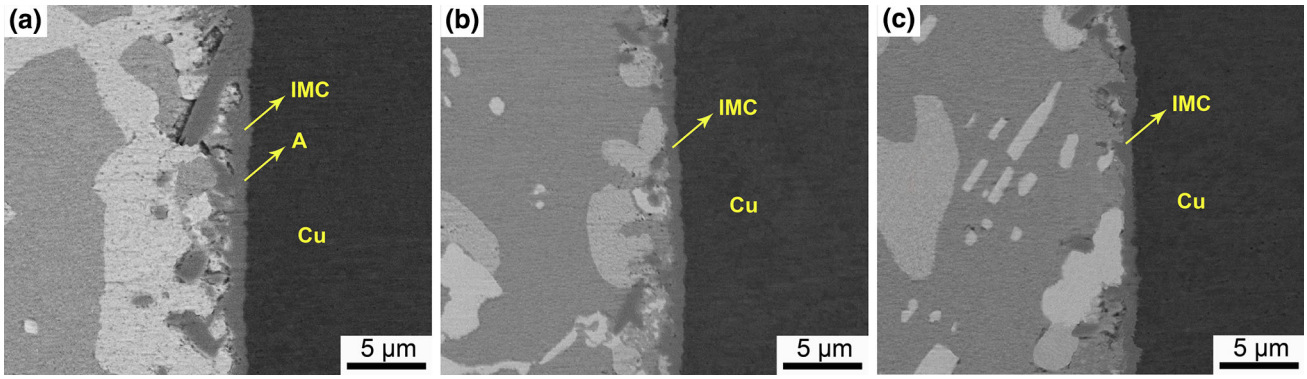


Fig. 5. Soldering interfaces for different compositions: (a) 38Sn-50Bi-12In, (b) 44Sn-44Bi-12In, and (c) 50Sn-38Bi-12In.

0.2 mm) for wetting experiments were ultrasonically cleaned in acetone followed by ethanol. Solder samples for wetting were about 0.2 g, and the testing temperature was 160°C with dwell time of 60 s. For one sample, the average spreading area of at least three tests was used to evaluate its wettability on Cu substrate.

The microhardness of samples was measured using an HXD-1000TMC/LCD microhardness tester, based on Vickers hardness with load of 25 g and dwell time of 10 s; the average value was obtained from more than seven indentations at different points on the sample surface.

Finally, tensile tests were conducted to measure the tensile strength and elongation of solder alloys and solder joints. The dimensions of the gage section of specimens for tensile tests are shown in Fig. 2. Tensile tests were conducted on a HT-2402 tensile testing machine at room temperature with loading speed of 1 mm/min; average values of tensile strength and elongation were estimated from five measurements. After the tensile tests, the fracture modes and morphologies of solder alloys and solder joints were analyzed by stereomicroscope and SEM, respectively.

## RESULTS AND DISCUSSION

### Microstructures of Solders and Solder Joints

Figure 3 shows the microstructures of Sn-Bi-In solders with various compositions; the corresponding EDX analysis results are presented in Table II.

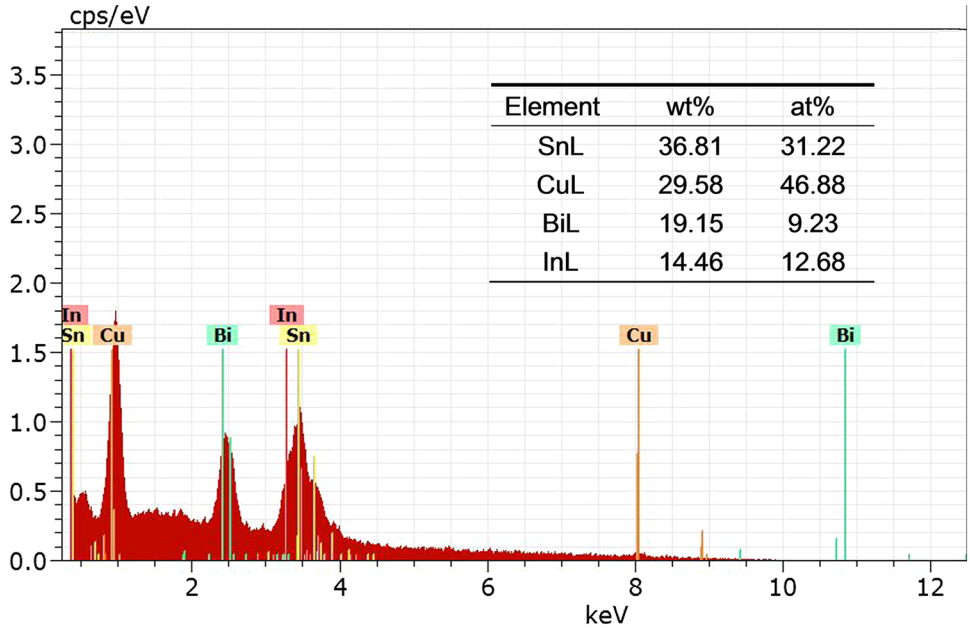


Fig. 6. EDX analysis for point A in Fig. 5.

**Table III. IMC thickness of solder joints**

| Alloy | IMC Thickness ($\mu$m) |
|---|---|
| 38Sn-50Bi-12In | 1.476 |
| 44Sn-44Bi-12In | 1.043 |
| 50Sn-38Bi-12In | 0.719 |

These results indicate that the microstructures are composed of dark InBi intermetallic phase, white Bi phase, and black $\beta$-Sn phase, consistent with results of previous study.[17] In addition, all these phases were confirmed by XRD intensity analysis, as shown in Fig. 4. No new intermetallic compound could be found in the microstructures of the investigated samples with different ratios of Sn and Bi elements.

According to the SEM results shown in Fig. 3, the proportion of Bi (white) phase in the micrographs reduced with decreasing Bi concentration. This is in agreement with the XRD profiles shown in Fig. 4, where the intensity of the corresponding characteristic peak for Bi phase decreases as the Bi content is reduced. The reason for precipitation of InBi secondary phase is that the solubility of InBi phase decreases obviously when the samples are cooled down to their eutectic point. Therefore, during solder solidification, InBi phase becomes increasingly supersaturated in $\beta$-Sn phase, and the supersaturation is relieved by formation of InBi intermetallic phase within the $\beta$-Sn phase.[18,23]

Figure 5 shows soldering interfaces for different compositions. During soldering, metallurgical reaction between the substrate and the molten solder can lead to formation of IMC at the interface. EDX was applied to analyze the composition distribution at the interface. Figure 6 indicates that the IMC layer was mainly composed of Sn and Cu elements, and it can be inferred from the results that $Cu_6Sn_5$ is the major intermetallic compound at the interface. In addition, the thickness of the IMC layer was calculated using ImageJ analysis software, as presented in Table III. These results show that, for lower Bi content, the total thickness of the IMC layer decreased, but not obviously so. Previous works[24,25] indicated that $Cu_6Sn_5$ IMC develops and $Cu_3Sn$ forms between $Cu_6Sn_5$ and Cu substrate. It has been reported that nanosized Bi particles segregate at the $Cu_3Sn$/Cu interface in solder joints,[26] and that Bi segregated at the $Cu_3Sn$/Cu interface can accelerate the $Cu_6Sn_5$ IMC growth rate in microelectronics interconnects.[27] With increasing Bi content, the Bi phase becomes prone to segregation at the interface, as shown in Fig. 5a, and the probability of Bi diffusion and segregation at the $Cu_3Sn$/Cu interface may be higher. This may slightly enhance the growth of the IMC layer.

## Melting Temperature Measurements

The melting temperature of the Sn-Bi-In solders was measured by DSC. The DSC results for the Sn-Bi-In solders with different compositions are shown in Fig. 7. A minor endothermic peak around 80°C to 84°C can be found on each curve. This peak is attributed to the solid-state phase transformation of InBi phase. The reaction is (Bi) + (Sn) + InBi $\rightarrow$ (Bi) + (Sn) according to vertical sections in the Bi-Sn-In system.[18,28] With increasing temperature, the InBi phase begins to disappear and indium atoms dissolve into the Bi and $\beta$-Sn phases. This ultimately leads to an enthalpy change. In addition, the

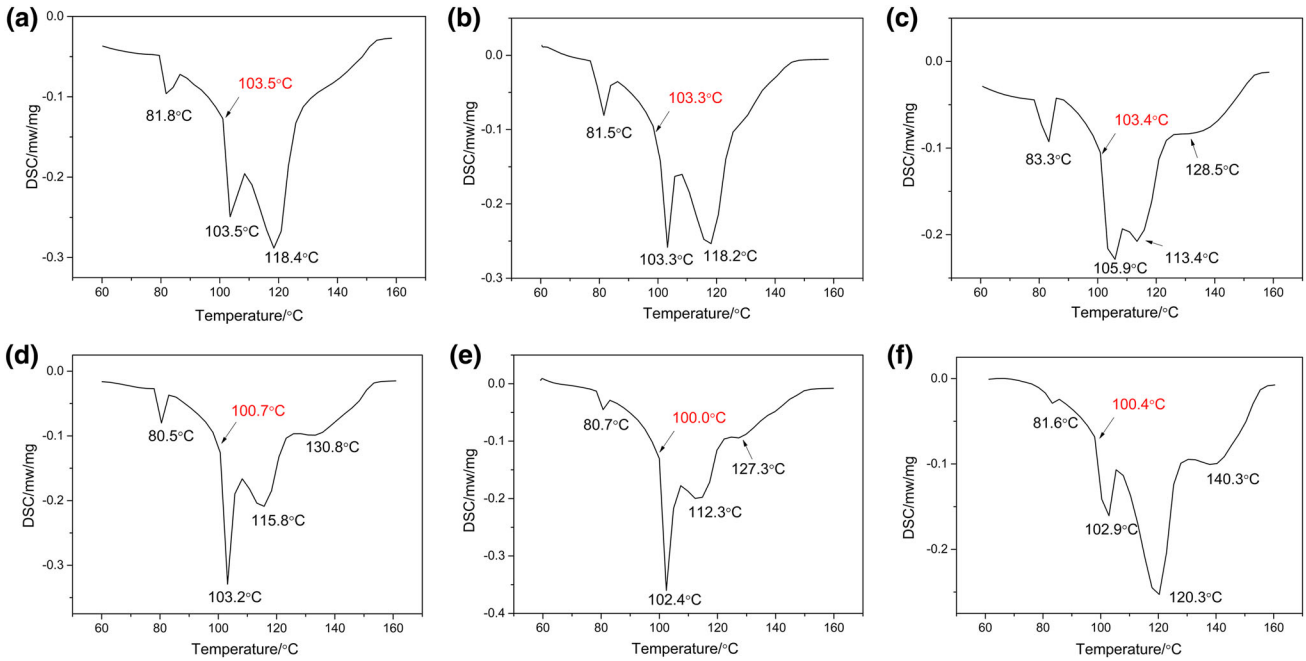


Fig. 7. DSC curves for various solder compositions: (a) 38Sn-50Bi-12In, (b) 41Sn-47Bi-12In, (c) 44Sn-44Bi-12In, (d) 47Sn-41Bi-12In, (e) 50Sn-38Bi-12In, and (f) 53Sn-35Bi-12In.

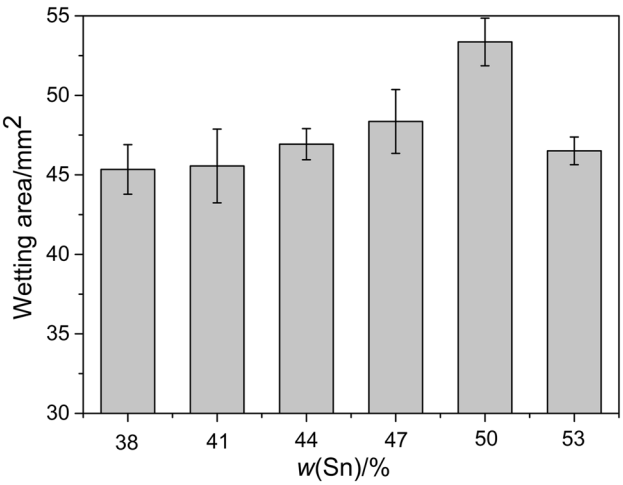


Fig. 8. Wetting area as a function of Sn concentration.

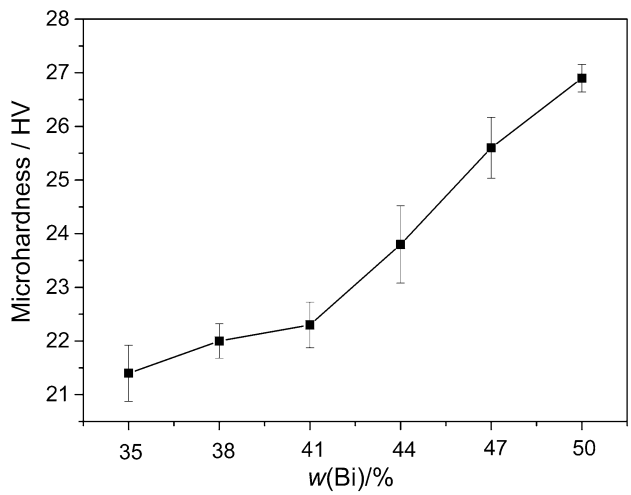


Fig. 9. Microhardness of solders as a function of Bi concentration.

peak value reduces with decreasing Bi concentration. This is because the binding between indium and bismuth atoms decreases with decreasing Bi content. Moreover, with reduction of the Bi content, the intensity of the corresponding characteristic peak for InBi phase in the XRD patterns shown in Fig. 4 also decreases. Both of these effects can lead to reduction of the InBi phase transformation and ultimately the endothermic peak value.

A notable endothermic peak at around 100°C to 104°C can be found for each of the compositions, and the reaction of Sn-Bi-In solders can be described as (Bi) + (Sn) → L(liquid) + (Bi) + (Sn)[17,18] during heating. This reaction indicates that the solders start to melt at these temperatures, which can be viewed as the onset melting temperatures (solidus temperatures), which are desired for low-temperature soldering. Moreover, all these temperatures are significantly lower than the Sn-Bi eutectic point due to the addition of pure indium ($T_m$ = 156.6°C), while variation of the Sn and Bi content has little effect on the onset melting temperature of the solders.

There is another major peak at around 113°C to 120°C on each DSC curve, which is attributed to

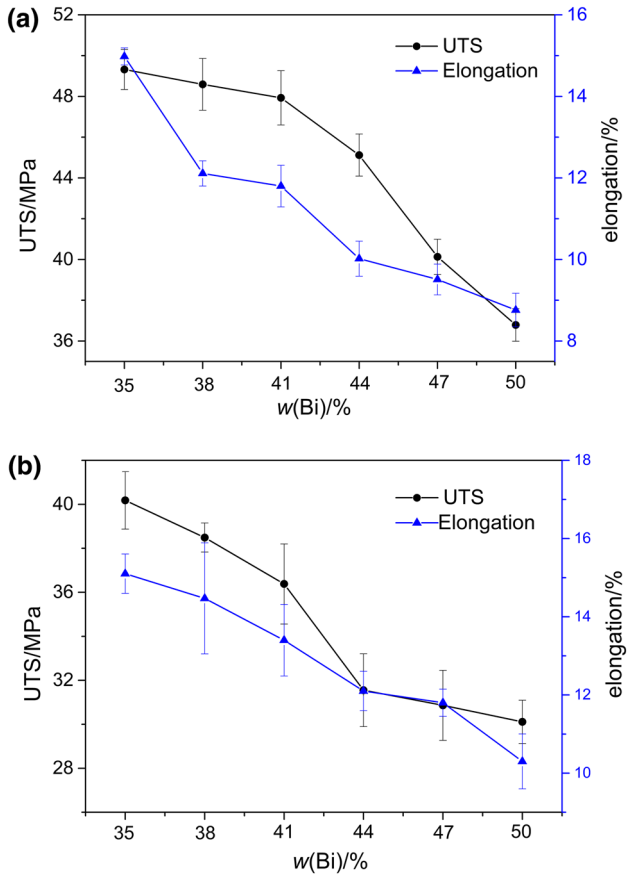


Fig. 10. Tensile strength and elongation of (a) solder alloys and (b) solder joints as a function of Bi concentration.

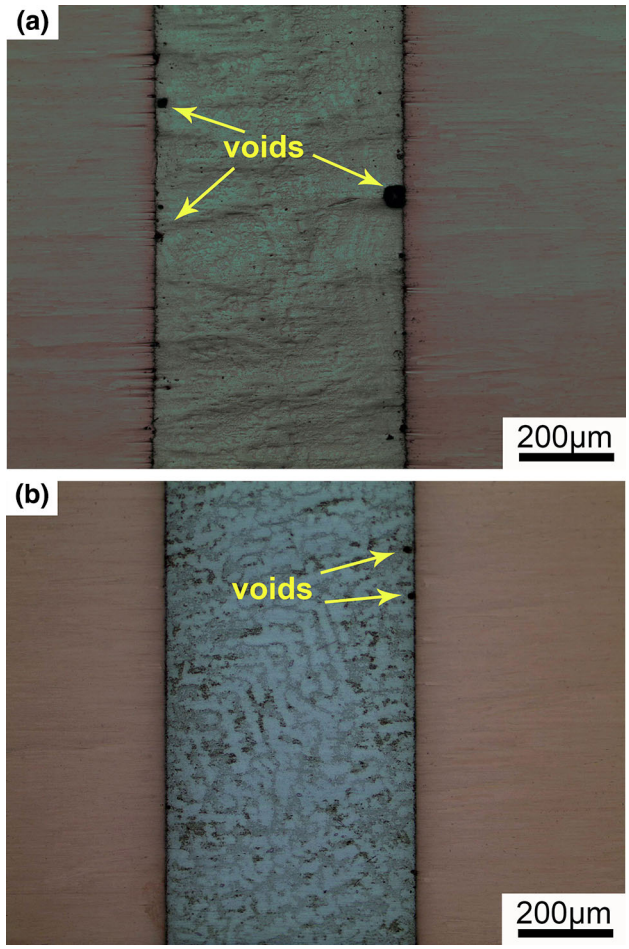


Fig. 11. Optical microscopy images of (a) 38Sn-50Bi-12In/Cu interface and (b) 53Sn-35Bi-12In/Cu interface.

melting of Bi phase in the solders during heating; the reaction is L + (Bi) + (Sn) → L + (Sn) according to the vertical sections through the Bi-Sn-In system calculated for 40 wt.% and 50 wt.% Sn.[17] In addition, with decreasing Bi content, the second major peak value reduces, as shown in Fig. 7a–e. These results agree well with the microstructures shown in Fig. 3, where the amount of Bi phase correspondingly decreases with decreasing Bi content. However, for the solder with 35 wt.% Bi content, the value of the second major peak is different from that on other DSC curves. This is caused by the mass ratio variation of Sn/Bi, according to the experimental data calculated by Scherpereel et al.[28] and the thermodynamic description elaborated by Witusiewicz et al.[18] These results indicate that, with increasing Sn/Bi mass ratio, the phase transformation becomes L + (Bi) + (Sn) → L + (Bi), which means that the $\beta$-Sn solid solution begins to melt when the temperature reaches 120°C. Meanwhile, the remaining Bi phase dissolves into the $\beta$-Sn phase, because the solubility of Bi solute in Sn matrix increases with temperature, reaching 21 wt.% at the eutectic point.[3] Moreover, the Sn content is apparently higher than the Bi content for the 53Sn-35Bi-12In solder in Fig. 7f, and the main component of the microstructure shown in Fig. 3f is $\beta$-Sn phase, thus the endothermic peak value of the phase transformation is larger than in the other DSC curves.

In addition, the third endothermic peak around 130°C becomes increasingly apparent as the Sn content is increased; the reaction is L + (Sn) → L, or $\beta$-Sn phase transformation. Meanwhile, the third peak in Fig. 7f is at around 140.3°C, close to the eutectic point of 139°C of Sn-Bi alloy. So a quasieutectic phase may form in the molten solder, causing the appearance of this peak as the temperature rises. All these temperatures can be viewed as liquidus temperatures.

Overall, it can be observed that the melting range first decreases and then increases with increasing Sn content, as seen in Fig. 7. A narrow melting range can ensure that the solder alloy exists as part liquid for a short time during solidification, forming reliable solder joints in the soldering process.[9] When the Sn content exceeded 50 wt.%, the melting range became wider, having a negative effect on solder joints in the soldering process.

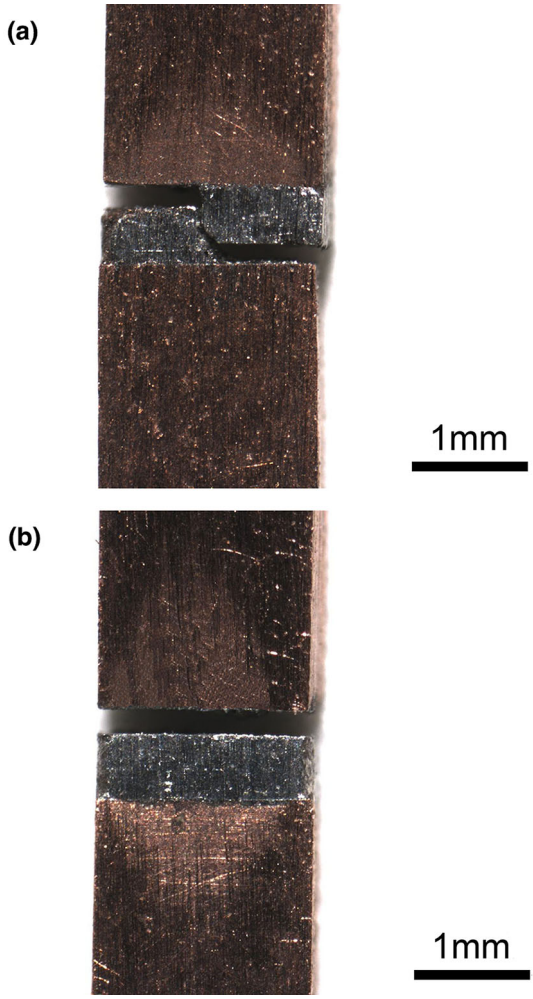


Fig. 12. Fracture modes of solder joints with different compositions: (a) 38Sn-50Bi-12In, (b) 53Sn-35Bi-12In.

## Wettability Properties

The wetting area of solders with various Sn compositions is shown in Fig. 8. On the condition that the Sn content is not beyond 50 wt.%, the wetting area increases with increasing Sn content. Cu atoms in the substrate can partly diffuse into the solder alloy, forming $Cu_6Sn_5$ with Sn element at the interface. For this reason, adding Sn element can improve the connection between the substrate and solder, thus improving the wettability. However, the wetting area remarkably decreased when the Sn content exceeded 50 wt.%; this is due to the strong reaction between Sn and Cu atoms at the interface when the Sn composition exceeds 50 wt.%. This restrains the spreading of the solder. In addition, the melting range becomes larger, as shown in Fig. 7f. This can also reduce the spreading and capillary flow of the molten alloy, ultimately resulting in poorer wettability. When designing Sn-Bi-In solders, a narrow melting range is required to obtain good solder wettability, thus the Sn composition should be controlled below 50 wt.%.

## Mechanical Properties

The results obtained from the microhardness tests on the Sn-Bi-In solders are shown in Fig. 9. It is indicated that the hardness of the solders decreased with reduction of the Bi concentration. Bismuth is a metal with hard and brittle properties. Its hardness is higher than the other elements in the Sn-Bi-In alloys. So, the hardness of the solders can be generally affected by the change of the Bi concentration. In addition, the Bi phase reduced with decreasing Bi content, as seen in Fig. 3; this leads to reduced microhardness. As revealed by Amares et al.,[29] the microhardness of Sn-Bi eutectic alloy is 11.8 $H_V$. However, the measured microhardness values of the Sn-Bi-In solders (Fig. 9) were apparently higher than that of Sn-Bi eutectic alloy. This may relate to the addition of In element. As discussed in the previous section, In atoms can dissolve into the Bi and $\beta$-Sn phases. This can induce solid-solution strengthening and increase the resistance to dislocation movement, thus enhancing the strength and hardness of the solder alloy. Besides, our experimental results show that the average hardness of InBi phase is 18.8 $H_V$. This also contributes to the microhardness improvement of the Sn-Bi-In solders compared with Sn-Bi eutectic alloy.

Figure 10 shows the tensile strength and elongation of the solder alloys and soldered joints as a function of the Bi concentration. The tensile strength of the solder alloys (Fig. 10a) declined with increasing Bi content. This is because a large amount of Bi atoms dissolving into the $\beta$-Sn phase can precipitate and grow into Bi phase with bulk or net-like shape on cooling to room temperature. Stress concentration occurs in the Bi phase during tensile deformation. In addition, the precipitated Bi phase can diffuse more easily and aggregate into coarse phases with increasing Bi content, thus causing the declining tensile strength of the solder alloys. For the solder joints, as the Bi content increases, the Bi phase tends to segregate at the interface, and the IMC layer becomes slightly thicker, as presented in Table III. Since the Bi phase and IMC layer in the soldered interface are hard and brittle, cracks occur more easily at the interface when the solder contains more Bi element. For this reason, the tensile strength of the solder joints also reduces with increasing Bi content.

It is indicated that the tensile strength of solder alloys was generally higher than that of solder joints for the same composition. There are several reasons to explain this phenomenon: One is that many voids formed along the solder/Cu substrate interface, as shown in Fig. 11. As the temperature was increased during soldering, flux between the

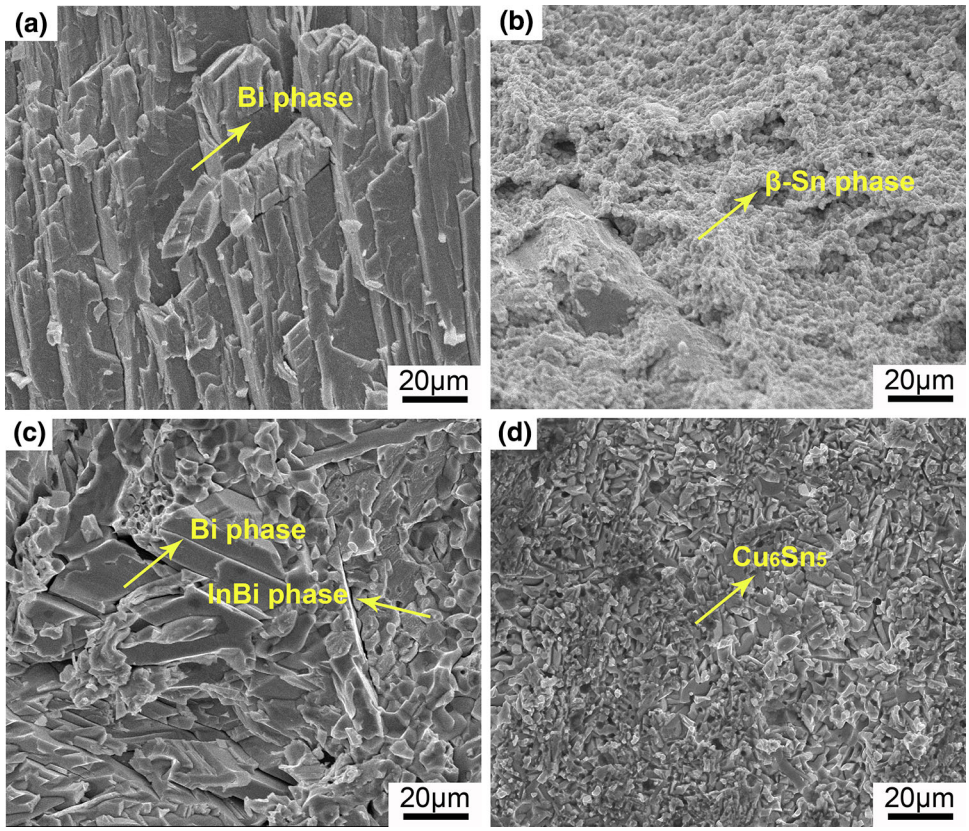


Fig. 13. Fracture surfaces of solder alloys: (a) 38Sn-50Bi-12In, (b) 53Sn-35Bi-12In, and solder joints (c) 38Sn-50Bi-12In/Cu, (d) 53Sn-35Bi-12In/Cu.

solder and Cu substrate begins to volatilize, due to the effect of flux activity. Bubbles can be generated in this reaction area, but their buoyancy cannot overcome the adhesive force with the Cu substrate during solidification,[30] resulting in voids at the interface. In addition, voids can not only act as a crack source but also reduce the active joint area under tension, which can ultimately affect solder joint reliability. Also, since the IMC layer has hard and brittle properties, cracks are easily generated at the IMC layer when samples suffer tensile stress. This may lead to solder joint failure. Overall, the tensile strength of the solder joints was lower than that of the solder alloys. It can also be observed that the tensile strength of the solder alloys and solder joints obviously dropped when the Bi content exceeded 41 wt.%. Therefore, Bi content of no more than 41 wt.% is recommended, considering the tensile strength of the solder.

The elongation of the solder alloys and solder joints declined with increasing Bi content, which is consistent with the variation of the tensile strength. The higher fraction of Bi phase seen in the micrographs can constrain the plastic deformation because slip planes cannot move freely in their preferred direction. This could lead to decreased elongation of the solder alloys. Also, the solder joints with higher Bi content had thicker IMC layer in the interconnects and Bi phase segregated at the interface, which could restrain the deformation of the solder joints and lead to a lack of ductility.

## Fracture Characteristics

Two fracture modes were observed in the solder joints with different compositions, as shown in Fig. 12. One type of failure occurred in both the solder and the IMC layer (solder/IMC mixed fracture mode). The other type occurred entirely in the IMC layer (IMC layer fracture mode). Because of the hard and brittle properties of Bi metal, solder joints with higher Bi content were prone to the mixed fracture mechanism when subjected to tension. The IMC layer fracture mode shown in Fig. 12b usually occurred for lower Bi content. Thus, the fracture mechanism is strongly affected by the Bi content.

To understand the effect of the failure behavior on the elongation, fracture surfaces of solder alloys after tensile tests are presented in Fig. 13a, b. It can be seen that the fracture morphology for higher Bi content (Fig. 13a) shows cleavage steps of different heights, obviously corresponding to brittle intergranular fracture. Meanwhile, for lower Bi content, the surface morphology was relatively smooth, and some dimples can even be seen in Fig. 13b. In addition, for higher Bi content, the fracture surface

was mostly composed of Bi phase, while the other case was mainly composed of $\beta$-Sn phase. This may be related to the double-layer flake rhombic structure of Bi crystal,[3] which makes solder deformation difficult. Thus, the elongation of the solder alloys (Fig. 10a) is greater for lower than higher Bi content.

It can also be observed in Fig. 13c and d that the fracture surface of solder joints exhibited rock shapes, while plastic deformation could hardly occur on the fracture surface. This indicates that the fracture mode of the solder joint generally corresponds to intergranular fracture or brittle fracture. Comparing these two images, the fracture surface for higher Bi content in Fig. 13c obviously shows cleavage steps and coarse grains. On the contrary, the crystal grains in the fracture surface for lower Bi content are relatively small and uniform. This can explain the result that the elongation of the solder joints (Fig. 10b) is lower when the solder contains more Bi element. In addition, with increasing Bi content in the solder, segregation of Bi phase would occur at interconnects as shown in Fig. 5a. Consequently, solder deformation is difficult under tension, and brittle fracture can easily occur at the interface of the solder joints. Besides, the fracture surface in Fig. 13c consists of Bi and InBi phases, while the other case mainly comprises $Cu_6Sn_5$, further illustrating the different fracture modes at the interface.

## CONCLUSIONS

The microstructures of the investigated Sn-Bi-In solders contained $\beta$-Sn, Bi, and InBi phases. The Bi phase content reduced with decreasing Bi content. The IMC layer at the Cu/solder interface was mainly composed of $Cu_6Sn_5$, becoming slightly thicker as the Bi content was increased.

Several endothermic peaks were found in the DSC curves: the solid-state phase transformation occurred at 80°C to 84°C on each DSC curve, and the onset melting temperature of the solders was seen at around 100°C to 104°C for low-temperature soldering. When the Sn content exceeded 50 wt.%, the melting range became wider and the wettability worse.

The microhardness of the Sn-Bi-In solders was higher than that of Sn-Bi eutectic alloy, also being enhanced by the presence of the element In. The tensile strength of the solder alloys and solder joints declined with increasing Bi content. Moreover, the former was generally higher than the latter for the same composition, being attributed to voids, Bi phase segregation, and brittle intermetallic compound at the interface.

For higher Bi content, solder joints exhibited the solder/IMC mixed fracture mode, whereas those with lower Bi content showed the IMC layer fracture mode. In addition, the fracture mechanism of the solder joints corresponded to brittle fracture; cleavage steps on the fracture surface and coarse grains in the fracture structures were comparatively apparent for higher Bi content, leading to lower elongation for both solder alloys and solder joints.

## ACKNOWLEDGEMENTS

The authors would like to gratefully acknowledge financial support from the National Natural Science Foundation of China (Grant No. 51275006), the Beijing Municipal Natural Science Foundation (Grant No. 3132006), and the Science Research Project of Beijing Municipal Education Commission (Grant No. KM2012100050010).

## REFERENCES

1. J. Chriašteľová and M. Ožvold, *J. Alloys Compd.* 457, 324 (2008).
2. L.R. Garcia, W.R. Osorio, L.C. Peixoto, and A. Garcia, *J. Electron. Mater.* 38, 2405 (2009).
3. Y.F. Yan and W.L. Wang, *Lead-Free Solders in Electronic Assembly (in Chinese)*, 1st ed. (Beijing: Publishing House of Electronics Industry, 2010), p. 41.
4. L. Zhang, S.B. Xue, L.L. Gao, Z. Sheng, H. Ye, Z.X. Xiao, G. Zeng, Y. Chen, and S.L. Yu, *J. Mater. Sci.* 21, 2 (2010).
5. S.K. Lin, T.L. Nguyen, S.C. Wu, and Y.H. Wang, *J. Alloys Compd.* 586, 319 (2013).
6. K. Suganuma and K.S. Kim, *J. Mater. Sci.* 18, 122 (2007).
7. X. Chen, J. Zhou, F. Xue, J. Bai, and Y. Yao, *J. Electron. Mater.* 44, 725 (2015).
8. Y. Shu, K. Rajathurai, F. Gao, Q.Z. Cui, and Z.Y. Gu, *J. Alloys Compd.* 626, 392 (2015).
9. J. Shen, Y.Y. Pu, H.G. Yin, and Q. Tang, *J. Electron. Mater.* 44, 532 (2015).
10. O. Mokhtari and H. Nishikawa, in *14th International Conference on Electronic Packaging Technology*, p. 251 (2013).
11. P.L. Liu and J.K. Shang, *Scr. Mater.* 44, 1020 (2001).
12. S. Sakuyama, T. Akamatsu, K. Uenishi, and T. Sato, in *Transactions of the Japan Institute of Electronics Packaging*, p. 99 (2009).
13. W.X. Dong, Y.W. Shi, Z.D. Xia, Y.P. Lei, and F. Guo, *J. Electron. Mater.* 37, 982 (2008).
14. F.W. Zhang, X.U. Jun, H.U. Qiang, H.E. Hui-Jun, and Z.G. Wang, *Chin. J. Nonferr. Met.* 19, 1782 (2009).
15. C. Zhang, S.D. Liu, G.T. Qian, J. Zhou, and F. Xue, *Trans. Nonferr. Metal Soc.* 24, 184 (2014).
16. T.H. Chuang and H.F. Wu, *J. Electron. Mater.* 40, 71 (2011).
17. S.W. Yoon, B.S. Rho, H.M. Lee, C.U. Kim, and B.J. Lee, *Metall. Mater. Trans. A* 30, 1503 (1999).
18. V.T. Witusiewicz, U. Hecht, B. Bottger, and S. Rex, *J. Alloys Compd.* 428, 115 (2007).
19. J.H. Wang, Y.Q. Yang, Q.Y. Li, S.C. Li, and Z.H. Liu, *Chin. J. Nonferr. Met.* 16, 1653 (2006).
20. E.E.M. Noor, A.B. Ismail, N.M. Sharif, T. Ariga, and Z. Hussain, in *33rd International Electronic Manufacturing Technology Conference*, p. 2 (2008).
21. O. Mokhtari and H. Nishikawa, *J. Electron. Mater.* 43, 4158 (2014).
22. Q. Li, Y.P. Lei, J. Lin, and S. Yang, in *16th International Conference on Electronic Packaging Technology*, p. 497 (2015).
23. D.R. Frear, S.N. Burchett, H.S. Morgan, and J.H. Lau, *The Mechanics of Solder Alloy Interconnects* (New York: Van Nostrand Reinhold, 1994), p. 8.
24. M.S. Park and R. Arróyave, *Acta Mater.* 60, 923 (2012).
25. C.C. Chang, Y.W. Lin, Y.W. Wang, and C.R. Kao, *J. Alloys Compd.* 492, 99 (2010).
26. C.Z. Liu and W. Zhang, *J. Mater. Sci.* 44, 149 (2009).

27. T.Y. Kang, Y.Y. Xiu, C.Z. Liu, L. Hui, J.J. Wang, and W.P. Tong, *J. Alloys Compd.* 509, 1785 (2011).
28. L.R. Scherpereel and E.A. Peretti, *J. Mater. Sci.* 2, 256 (1967).
29. S. Amares, M.N.E. Efzan, and T.C. Yap, *Adv. Mater. Res.* 845, 261 (2014).
30. W.B. Hance and N.C. Lee, *Solder Surf. Mt. Tech.* 5, 16 (1989).